Microbiome

RESEARCH

Open Access

Microbiota-derived urolithin A in monoclonal gammopathies and multiple myeloma therapy

Alba Rodríguez-García[1*], Raquel Ancos-Pintado[1,2†], Roberto García-Vicente[1†], Alejandra Ortiz-Ruiz[1], Andrés Arroyo[1], Miguel Ángel Navarro[1], María Luz Morales[1], Patricia Guevara-Ramirez[1], Pablo Justo[1], Nieves López-Muñoz[1], José Sánchez-Pina[1], Rafael Alonso[1], María Victoria Selma[3], María Dolores Frutos-Lisón[3], Rocío García-Villalba[3], Francisco A. Tomás-Barberán[3], Rosa Ayala[1,4], Joaquín Martínez-López[1,4†] and María Linares[1,2*†]

Abstract

Background Gut microbiota-derived urolithins may influence multiple myeloma (MM) disease progression and treatment. We analyzed urolithins and their associated microbiota in a retrospective cohort of 45 patients with active MM or premalignant disease using mass spectrometry and 16S rRNA gene sequencing.

Results Patients with detectable levels of urolithin in serum and stool and a higher abundance of urolithin-related microbiota had a better outcome. Analysis of the effects of urolithin A (UroA) treatment ex vivo, in vitro, and in vivo revealed that UroA is cytotoxic against MM cell lines and modulates the cell cycle and mitochondrial activity. Notably, UroA inhibits the proliferation of primary MM cells in vitro and in a xenograft mouse model, improving overall survival. Finally, combination therapy with UroA and bortezomib has a synergistic effect in vitro, even in the presence of bortezomib resistance, and modulates signaling pathways involved in MM development.

Conclusions UroA might be a potential therapeutic agent to halt MM disease progression or to overcome resistance when used in combination.

Keywords Multiple myeloma, Gut microbiota, Urolithin, Metabolites

†Raquel Ancos-Pintado and Roberto García-Vicente contributed equally as second authors.

†Joaquín Martínez-López and María Linares contributed equally as co-senior authors.

*Correspondence:
Alba Rodríguez-García
albarodriguezgarcia@hotmail.com
María Linares
mlinares@ucm.es
[1] Hematological Malignancies Clinical Research CRIS Unit H120-CNIO, Department of Hematology, Hospital Universitario 12 de Octubre, imas12, Universidad Complutense de Madrid, Madrid, Spain
[2] Department of Biochemistry and Molecular Biology, Pharmacy School, Universidad Complutense de Madrid, Madrid, Spain
[3] Laboratory of Quality, Safety, and Bioactivity of Plant Foods, CEBAS-CSIC, Murcia, Spain
[4] Department of Medicine, Medicine School, Universidad Complutense de Madrid, Madrid, Spain

Introduction

Multiple myeloma (MM) is a common type of blood cancer characterized by the abnormal growth of plasma cells in the bone marrow (BM) and belongs to a class of disorders known as the monoclonal gammopathies [1]. MM is a progressive disease that is preceded by an asymptomatic stage known as monoclonal gammopathy of undetermined significance (MGUS) and also often by an intermediate stage known as smoldering myeloma (SMM) [1–5]. Approximately, 15% of patients with MGUS and 10% with SMM will progress to MM within the first 5 years from diagnosis [1, 2]. Despite recent advances in the treatment of MM with proteasome inhibitors, immunomodulatory drugs, and CD38-targeting antibodies, the disease remains incurable [6]. Achieving a complete response to therapy improves long-term survival, but disease progression and relapse are marked by increased treatment resistance [6].

Several studies have suggested an association between MM and viral infections, particularly hepatitis B and C viruses, human immunodeficiency virus, and Epstein-Barr virus [2–9]. The gut microbiota, consisting of microorganisms in the intestinal tract, is crucial in the pathogenesis of some cancers [10, 11]. An imbalance in the composition of the microbiota, termed dysbiosis, disrupts the interaction between microorganisms and host epithelial/immune cells, leading to disturbances in inflammation, immune regulation, cell cycle, proliferation, and mucus production [10]. A growing body of research has focused on understanding the role of the gut microbiota in MM progression [12–17], and some specific microorganisms have been found to promote the differentiation and migration of immune cells from the gut to the BM, thereby favoring MM progression [13]. The nature of the gut microbiota also influences the antigenic stimulation of plasma cells in MM, potentially contributing to the emergence of new mutations and clonal evolution. Indeed, pathogenic species of the gut microbiota have been suggested to cause antigenic stimulation in the premalignant stage (MGUS) and in MM, highlighting the influence of the gut microbiota on the myeloma microenvironment [8, 18].

The gut microbiota also serves as a reservoir of myriad metabolites derived from dietary components and host metabolism [19]. These metabolites, particularly bacterial metabolites, play an important role in microbiota–host interactions and influence the immune system and the BM microenvironment. Some of these metabolites may have a beneficial effect on MM outcomes [20]. For example, we recently reported that short-chain fatty acids produced by the gut microbiota are associated with response and improved survival in MM [21].

The urolithins are a group of dietary metabolites produced by the gut microbiota and derived from ellagitannins found in various foods such as berries (raspberries, blackberries, strawberries), pomegranates, tea, nuts, and oak-aged wines [22–24]. Among the urolithins, urolithin A (UroA, 3,8-dihydroxyurolithin) is considered to be the most biologically active and is highly conserved across species [22, 23]. UroA has been shown to influence several biological processes including the regulation of oxidation, inflammation, cancer, obesity, and aging [23, 25]. One of its more well-studied mechanisms of action is the improvement of mitochondrial function and mitochondrial oxidative phosphorylation [26, 27], which is dysregulated in hematological tumors including MM [28].

UroA also has anticancer properties and has been shown to regulate the expression of multiple genes involved in oncogenesis, cell cycle regulation, tumor suppression, and growth factor signaling [23, 29–31]. For example, it can induce cell cycle arrest in cancer cells and inhibit the PI3K/AKT/mTOR pathway, which has been linked to several cancers including MM [30]. In addition, in vitro studies have demonstrated its anticancer effects in human cell models of prostate, liver, breast, colon, and pancreatic and endometrial cancer [25].

Although research on urolithins, particularly UroA, in the context of MM is limited, existing evidence from other cancers suggests that further investigation of their effects on MM development and progression is warranted. Understanding the interplay between the gut microbiota, urolithins and MM may pave the way for novel therapeutic strategies targeting the microbiota and its metabolites in the management of this hematological malignancy. The aim of the present study was to investigate urolithin production by the gut microbiota and its potential impact on the prevention of MGUS progression, as well as on the prognosis and treatment of MM. Additionally, we investigated the therapeutic effects of UroA on pathological plasma cells and explored the underlying pathways.

Materials and methods

Patients and sample collection

A retrospective cohort of 45 patients from Hospital 12 de Octubre (Madrid, Spain) with MGUS ($n=11$), SMM ($n=8$), newly diagnosis MM (NDMM) ($n=15$), MM at relapse or refractory disease (RRMM) ($n=7$), and MM at complete remission (CRMM) ($n=8$, 4 paired samples) were included in the study. The inclusion criteria were confirmed diagnosis of MGUS, SMM, NDMM, RRMM or CRMM, sufficient availability of stool, serum, and/or bone marrow samples, as well as participants' willingness to take part in the study. The control group ($n=8$, median age 66 years; range 49–94 years) consisted of the

relatives of the study population of similar age and habits and with no signs of the disease in the BM to minimize bias. For microbiota and urolithins detection, fecal and serum samples of 40 patients were collected between 2018 and 2021 and processed as described [21]. The clinical characteristics of participants for these studies at the time of diagnosis are shown in Supplementary Table S1. For ex vivo assays, 5 MM patients with > 8% of plasma cells (by flow cytometry analysis of BM) were used.

Sequencing and bioinformatics analysis

Patients provided stool samples in sterile containers. Upon delivery to the hospital, the samples were promptly aliquoted and stored at − 80 °C for future analysis. Microbial DNA was extracted from 200 mg of stool using the AllPrep PowerFecal DNA/RNA Kit (QIAGEN, Hilden, Germany), and DNA concentration was measured with a Qubit 4.0 Fluorometer utilizing the dsDNA HS Assay (Thermo Fisher Scientific, Waltham, MA, USA). The ZymoBIOMICS® Microbial Community Standard was used as positive control; a blank extraction sample was used as a negative control. Bacterial 16S rRNA gene sequencing was performed on the Illumina® MiSeq™ platform (Illumina Inc., San Diego, CA, USA) as described [21]. Briefly, libraries were prepared using Quick-16S NGS Library Prep Kit (Zymo Research). The bacterial 16S primers amplified the V3–V4 regions of the 16S rRNA gene. Primers were custom-designed by Zymo Research to provide the best coverage of the 16S gene while maintaining high sensitivity. Final library was sequenced on an Illumina MiSeq instrument (RRID:SCR_016379) using the v3 reagent kit (600 cycles). The sequencing was performed with > 10% PhiX spike-in.

Microbiome bioinformatics analysis was performed with QIIME 2 [32]. Demultiplexed paired-end sequencing raw data were processed, with initial preprocessing steps including quality control and sample count summarization performed using the q2-demux plug-in. Sequence denoising was performed with DADA2 [33], employing the *denoise-paired* function optimized for paired-end reads (via q2-dada2). This process encompassed primer sequence removal, low-quality region trimming, dereplication, read merging, chimera filtering, and singleton removal, resulting in an amplicon sequence variant (ASV) feature table. Primer sequences were removed by specifying the following parameters: *--p-trim-left-f 16*, *--p-trim-left-r 24*, *--p-trunc-len-f 280*, and *--p-trunc-len-r 240*.

To ensure data quality, ASVs with a total frequency of fewer than 2 reads were filtered out using the *qiime feature-table filter-features* command with the *--p-min-frequency 2* parameter. Since 5621 reads represented the lowest read depth, no samples were excluded. Subsequently, ASVs were clustered into operational taxonomic units (OTUs) at 99% similarity using a closed-reference approach with the SILVA 138 Ref. NR 99 [34] database and the *qiime vsearch cluster-features-closed-reference function* [35] with the *--p-perc-identity 0.99* parameter.

Alpha diversity was calculated by rarefying all samples to the minimum read depth of 5621 reads. The following metrics were computed using the *diversity.alpha* module of the *scikit-bio* Python library: Chao1, Shannon, Simpson, and Pielou's evenness.

Differential abundance analysis was conducted on the genus-level OTU table, after collapsing using *qiime taxa collapse* command, to identify potential biomarkers between study conditions. OTU counts were normalized to relative abundances by total sample counts. Biomarker identification was carried out using linear discriminant analysis effect size (LEfSe, v1.1.2) [36], with an adjusted *p*-value (Benjamini–Hochberg) threshold of < 0.05 and an absolute LDA score > 2.5 to classify taxa as differentially abundant between the groups of interest. Differential abundance results were visualized using the LEfSe graphical output option, and the relative abundances of taxa of interest were plotted using GraphPad Prism (v8.0.1.).

Liquid chromatography-mass spectrometry analysis

Fecal samples (300 mg) were defrosted and homogenized with 10 mL of MeOH/DMSO/H2O (40:40:20) and 0.1% HCl using the Vibra-Cell VC 50 Ultrasonic Homogenizer (Danbury, CT, USA) for 1 min. The mixture was centrifuged at 5000 × *g* for 10 min at room temperature, and the supernatant was filtered through a 0.22-µm PVDF filter before analysis [37].

Urolithins were determined in feces as urolithin glucuronide and sulfates as well as the aglycones conjugates as previously reported by García-Villalba et al. [38]. Analyses were performed on an HPLC chromatograph (1200 Series, Agilent Technologies Inc., Santa Clara, CA, USA) coupled to a single quadrupole mass spectrometer detector and a diode-array detector in series (6120 Quadrupole, Agilent Technologies). Urolithins were identified using their UV spectral properties and molecular mass and by comparison with authentic standards available in the CEBAS-CSIC metabolites collection (Murcia, Spain). In patients with detectable levels of urolithins, the type of urolithin detected and the metabotype were also determined (see Supplementary Table S2).

Serum samples (200 µL) were thawed and extracted with 600-µL acetonitrile:formic acid (98:2, v/v) by vortexing for 2 min and ultrasonic bath for 10 min. The mixture was centrifuged at 14000 × g for 10 min, and the supernatant was reduced to dryness in the speed vacuum concentrator (Savant SPD121P, Thermo Scientific,

Alcobendas, Spain). The dried samples were resuspended in 100 µL of MeOH and filtered through a 0.22-µm PVDF filter before analysis.

Serum samples were analyzed in an Agilent 1290 Infinity UPLC system coupled to a 6460 Triple Quadrupole (QqQ) mass spectrometer (Agilent Technologies, Santa Clara, CA, USA) using the chromatographic and mass spectrometry conditions previously optimized [38]. The optimized MRM transitions were as follows: Uro-A glucuronide and isoUro-A glucuronide (403 > 227; 403 > 113); Uro-A sulfate (307 > 227; 307 > 198); Uro A (227 > 198; 227 > 182); Uro-B glucuronide (387 > 211; 387 > 113); and Uro-B sulfate (291 > 211; 291 > 167). Each urolithin was quantified with its own standard.

Cell lines

JJN3 and U266 and cell lines were directly obtained from the DSMZ repository (Braunschweig, Germany). RPMI-8226, XG-1, and ARP-1 cell lines were provided by Dr. Antonio Valeri (Hospital 12 de Octubre, Spain), Dr. Shelly Lawson (Sheffield University, UK), and Dr. Joshua Epstein (Arkansas Cancer Research Center, AR, USA), respectively. JJN3 and U266 lines were previously modified in our laboratory with green fluorescent protein and luciferase. A bortezomib-resistant JJN3 cell line (JJN3_R-Btz) was established by dose escalation of the drug once weekly up to a dose of 11 nM. All cells were cultured in RPMI-1640 medium (Biowest, Nuaillé, France) supplemented with 10% fetal bovine serum and 1% penicillin–streptomycin at 37 °C in a humidified incubator at 5% CO_2 and were passaged every 2–3 days.

In vitro and ex vivo drug assays

The effect of UroA (ref. 4C28139, 1Click Chemistry Inc., NJ, USA), bortezomib (ref. S1013, Selleckchem, TX, USA), lenalidomide (ref. HY-A0003, MedChemExpress, NJ, USA), and venetoclax (ref. S8048, Selleckchem, TX, USA) on cell viability was assessed in MM cell lines (JJN3, JJN3_R-Btz, U266, RPMI-8226, XG-1, and ARP-1 cell lines) and peripheral blood mononuclear cells (PBMCs) from healthy donors and non-transformed T cells. Cells were seeded at 5×10^5 cells/mL for cell lines and 1.5×10^6 cells/mL for primary cells and treated for 48 h with UroA in monotherapy, in combination with bortezomib, or with vehicle (DMSO). Cell viability was determined using the Cell Counting Kit-8 Reagent (Sigma-Aldrich, St. Louis, MO, USA) on an Epoch microplate reader running Gen5 2.0 software (BioTek Instruments, Winooski, VT, USA). For in vitro monotherapy treatments, percentage cell survival from three independent experiments was calculated and normalized to controls. Half-maximal inhibitory concentration (IC_{50}) values were determined according to a nonlinear regression program (GraphPad Software Inc., La Jolla, CA, USA), and dose–response graphics were represented as the mean survival ± standard error of the mean (SEM). For in vitro combinational treatments, drug effects from three independent experiments were tested, and the combination index (CI) was calculated. Drug synergism, addition, and antagonism effects were defined by CI values of < 1.0, 1.0, and > 1.0, respectively. The Chou-Talalay Combination Index Theorem [39] was used to calculate the CI of bortezomib and UroA.

For ex vivo assays, erythrocyte-lysed whole BM mononuclear cells (BMMCs) were studied by flow cytometry. All events from the distinct conditions applied to BMMCs were analyzed, with 5×10^4 events for each condition. The plasma cell population (CD38 + CD138 +) was assessed to detect variations after treatment with UroA (15 µM and 30 µM) compared with vehicle-treated cells. Before acquisition, cells were incubated for 30 min at room temperature with CD38-FITC (BD Biosciences, Franklin Lakes, NJ, USA) and CD138-PECy7 (BioLegend, San Diego, CA, USA).

Western blotting

After treatment with bortezomib (4 nM), UroA (15 µM), their combination, or vehicle (as a control), cells were lysed and cleared by centrifugation (14,000 × *g*, 4 °C, 5 min), and the protein concentration was determined with the Quick Start™ Bradford 1 × Dye Reagent (Bio-Rad Laboratories, Hercules, CA, USA) on the Epoch microplate reader. Equal amounts of proteins were separated on 10% SDS-PAGE gels and transferred to PVDF Immun-Blot membranes (Bio-Rad Laboratories). Blots were incubated with primary and secondary antibodies (see Supplementary Table S4). An antibody for GAPDH was used to check for equivalent protein loading. Membranes were developed by enhanced chemiluminescence (Clarity Western ECL Substrate; Bio-Rad Laboratories), and protein bands were detected with a ChemiDoc MP instrument (Bio-Rad Laboratories). Densitometry was performed using Image Lab 5.0 software (Bio-Rad Laboratories), normalized to the signal of GAPDH and normalized to the control.

Quantitative PCR

After treatment with bortezomib (4 nM), UroA (15 µM), their combination, or vehicle (as a control), cells were lysed and cleared by centrifugation (14,000 × *g*, 4 °C, 5 min). cDNA synthesis from extracted RNA was performed with the High-Capacity cDNA Reverse Transcription Kit (Thermo Fisher Scientific, Waltham, MA, USA) on the Veriti 96-Well Thermal Cycler platform (Applied Biosystems, Foster City, CA, USA), maintaining a 1:1 ratio of reverse transcriptase buffer and RNA.

Gene expression levels of p21 (ref. Hs00355782_m1) and the constitutive gene β-glucuronidase (GUS) (ref. Hs00939627_m1) gene were measured following the TaqMan® Gene Expression Assay protocol provided by Thermo Fisher. All samples were tested in triplicate, and the changes in gene expression were calculated using the comparative ΔCT method [40]. Expression levels were normalized to those of control samples.

Cell cycle analysis

The JJN3 cell line (5×10^5 cells/mL) was exposed to 15-μM UroA or vehicle only for 24 h, after which time 1×10^6 cells were harvested, washed with PBS, and fixed and permeabilized with cold 70% ethanol overnight at − 20 °C. Cells were then washed twice with PBS and incubated for 30 min in the dark at room temperature with 10-μL propidium iodide and 2.5-μL RNAase A (ref. 10109142001; Merck Millipore, Darmstadt, Germany) in PBS to a final volume of 250 μL. After centrifugation and resuspension in PBS, cells were analyzed on the FACSCanto II flow cytometer (BD Biosciences). Data collection was done with FACSDiva software (BD Biosciences) on 3×10^4 events per condition. Results were analyzed with FlowJo™ version 10 (BD Biosciences).

Immunocytochemistry analysis

JJN3 cells were treated with different doses of UroA (15 μM, 30 μM, 60 μM, or 100 μM) or vehicle for 48 h and then fixed with methanol. Immunocytochemistry analysis was performed as described [41]. Briefly, slides were refreshed in 1% bovine serum albumin in PBS, and endogenous peroxidase was inactivated with 3% hydrogen peroxide for 5 min. Antigen unmasking and recovery were performed by heat-mediated antigen retrieval with citrate buffer. 4-Hydroxynonenal (HNE) adducts were detected using an anti-4-HNE rabbit antibody (1:100 dilution, ref. ab46545, Abcam, Cambridge, UK). Slides were counterstained with Carazzi's hematoxylin solution, dehydrated in an ethanol series (100%, 96%), and cleared in xylol and mounted with DPX mounting medium (Sigma-Aldrich). Samples were visualized and imaged using a Nikon Eclipse 80i microscope (Tokyo, Japan) equipped with a Nikon digital camera.

Animal model

A MM xenograft mouse model was used for the in vivo study, which was conducted according to the guidelines of the Institutional Animal Care and Use Committees of the Comunidad de Madrid, Spain, using an approved protocol (PROEX 023/17). Female 6–8-week-old NOD.Cg-Prkdcscid Il2rgtm1Wjl/SzJ (NSG) mice (Charles River Laboratories, Madrid, Spain) were inoculated intravenously by tail vein injection with JJN3 cells (1×10^6). Three days later, mice were randomized into two groups of five animals: one group received an intraperitoneal injection of vehicle (DMSO) 5 days a week; the other group received UroA 200 mg/kg body weight intraperitoneally five times weekly. Mice were monitored weekly for 4 weeks for tumor burden, distribution, and engraftment by whole-body bioluminescence imaging using the IVIS Imaging system (Caliper Life Sciences, Hopkinton, MA, USA). Before acquisition, 150 mg/kg body weight of luciferin (D-luciferin monosodium salt, Thermo Fisher) prepared in PBS was injected intraperitoneally, followed by luminescence signal detection 10 min later. The signal data were analyzed using Living Image 4.2 software (Caliper Life Sciences).

Statistical analysis

Descriptive analyses of clinical variables were stratified by disease stage. Categorical variables were expressed as percentages, while numerical variables were reported as median and range. Statistical comparisons were performed using either the parametric Student's *t*-test or the nonparametric Mann–Whitney *U*-test, based on the data distribution. Differences in the frequencies of disease stages between patients with detectable urolithins or not detectable urolithins were assessed using Fisher's exact test. In vitro experiments were conducted in triplicate for each condition. Survival analysis was conducted using the Kaplan–Meier method with the log-rank test. A P-value < 0.05 was considered statistically significant. All statistical analyses and data visualizations were carried out using GraphPad Prism (v8.0.1.) or R Studio (v4.4.1) [42].

Results

Urolithin levels and urolithin-related microbiota are decreased in patients with active MM and correlate with survival

We first investigated whether the progression of MM from premalignant stages (MGUS and SMM) and its response to pharmacological treatment were influenced by urolithin levels. We classified patients according to whether or not they had detectable urolithin levels in stool and found that none of the patients with relapse (RRMM) had detectable urolithin (Fig. 1A). In patients with detectable levels of urolithin, 15% had active disease compared with 62% with pre-MM and 23% with complete remission (CRMM) ($P=0.043$). Contrastingly, 56% of patients with undetectable levels of urolithins had active MM compared with 36% of patients with pre-MM and 8% with CRMM (Fig. 1B). These results were also observed when studying UroA in serum samples (Supplementary Fig. 1A and B). We questioned whether the presence of urolithin was related to patient survival,

finding superior progression-free survival ($P=0.05$) in patients after receiving treatment (CRMM and RRMM) with detectable levels of urolithins (Fig. 1C).

Because greater gut microbiota alpha diversity has been associated with greater urolithin production in health and in disease states such as Parkinson's disease [43], we examined alpha diversity and its relationship to urolithin production in patients with MM. Results showed that the main alpha-diversity indices (Chao, Pielou, Shannon, and Simpson) were significantly higher in those patients with detectable levels of urolithins (Supplementary Fig. 1C, D, E, F). In a previous study [21], we investigated specific changes in the gut microbiota using the LEfSE biomarker discovery tool, which identifies the genera that drive the divergence between control and MM at different stages (Supplementary Fig. 2A). Based on this analysis, we found that some genera of the Eggerthellaceae family such as *Raoultibacter*, *Senegallimassilia*, and *Adlercreutzia (*previously named *Enterorhabdus)* were enriched in the control group when compared with the NDMM group. These genera are phylogenetic neighbors of bacteria recognized as urolithin producers such as *Gordonibacter* and *Ellagibacter* [44]. By contrast, *Erysipelatoclostridium* was more abundant in the NDMM group than in the control group (Supplementary Fig. 2B) and has been shown to inversely correlate with urolithin levels [45]. *Ruminococcus* has been shown to positively correlate with urolithin production [46], and we found a lower abundance of this genus at relapse (RRMM); conversely, *Phocea* negatively correlates with urolithin levels [45] and was greater in abundance at this stage *versus* NDMM (Supplementary Fig. 2C). When comparing treatment responses, LEfSE analysis identified *Terrisporobacter* as a biomarker of CRMM (Fig. 1D), showing a significantly higher abundance in CRMM compared to RRMM (Fig. 1E). Also, this genus was a biomarker of NDMM when compared with RRMM (Supplementary Fig. 2A). Of note, this genus is associated with the production of a greater number of urolithins, including UroA, IsoUroA, and UroB [45, 47]. Moreover, patients with *Terrisporobacter* had a superior survival rate than those who did not ($P=0.04$) (Fig. 1F).

UroA treatment inhibits proliferation and cell cycle progression of MM cell lines

To evaluate the possible cytotoxic effect of UroA in MM cell lines, we tested the survival of JJN3 and U266 cells after exposure to a range of UroA concentrations for 48 h. As shown in Fig. 2A, UroA was cytotoxic in both cell lines with IC_{50} values in the lower micromolar range (IC_{50} JJN3: 6.99, 95% confidence interval [CI] 5.14–9.52 μM; IC_{50} U266: 16.51, 95% *CI* 11.72–23.24 μM). These effects were reproduced in other three MM cell lines (IC_{50} RPMI-8226: 2.93, 95% *CI* 1.09–7.82 μM; IC_{50} XG-1: 4.43, 95% *CI* 3.26–6.03 μM, and IC_{50} ARP-1: 14.42, 95% *CI* 11.17–18.63 μM). Since the JJN3 cell line showed an intermediate IC50 value compared to the others, we decided to proceed with this line for the subsequent assays. As expected, the inhibition of proliferation by UroA was accompanied by cell cycle arrest, as evidenced by an increase in the number of cells in S ($P=0.001$) and G2/M ($P=0.01$) phases and a decrease in cells in the G0/G1 phase ($P=0.04$) as compared with control conditions (Fig. 2B). In line with these results, an increase in p27, BAX (Fig. 2C), p53, and p21 (Supplementary Fig. 5A and B) was observed.

UroA treatment decreases mitochondrial respiratory chain content and attenuates oxidative stress in MM cell lines

Given the established functional link between urolithins and mitochondrial activity [26, 27], we investigated the protein expression of respiratory chain complexes in myeloma cells after exposure to 15-μM UroA for 48 h. Results showed that the levels of mitochondrial complexes III, IV, and V were significantly lower ($P=0.05$) in JJN3 cells treated with UroA than in vehicle-treated cells (Fig. 3A). To study the impact of UroA on oxidative stress, we measured the levels of 4-hydroxynonenal (HNE) as a metric of lipid peroxidation. Immunocytochemistry analysis of JJN3 cells revealed a decrease in HNE labeling across a range of UroA concentrations from 15 to 100 μM (Fig. 3B). This was accompanied by an increase in expression of the antioxidant mediator NRF2 (Fig. 3C).

(See figure on next page.)

Fig. 1 **A** Proportion (%) of patients with monoclonal gammopathy of undetermined significance (MGUS), smoldering myeloma (SMM), new diagnosed MM (NDMM), MM in complete remission (CRMM), and at relapse/refractory (RRMM) with detectable or undetectable levels of urolithins in stool. **B** Proportion (%) of patients with premalignant disease (MGUS and SMM), active MM (NDMM and RRMM), and CRMM with detectable or undetectable levels of urolithins in stool. **C** Representation of the Kaplan–Meier progression-free survival probability (PFS) in patients after receiving treatment (CRMM and RRMM) with undetectable (red) or detectable (blue) stool urolithins. **D** Taxonomic biomarkers identified by LEfSe analysis between patients with RRMM and CRMM. **E** Relative abundance (%) of the genus *Terrisporobacter* in patients with CRMM and RRMM. **F** Representation of the Kaplan–Meier overall survival probability (OS) of treated patients (RRMM and CRMM) with undetectable (red) or detectable (blue) stool levels of *Terrisporobacter*. $^{*}P \leq 0.05$; $^{**}P \leq 0.01$

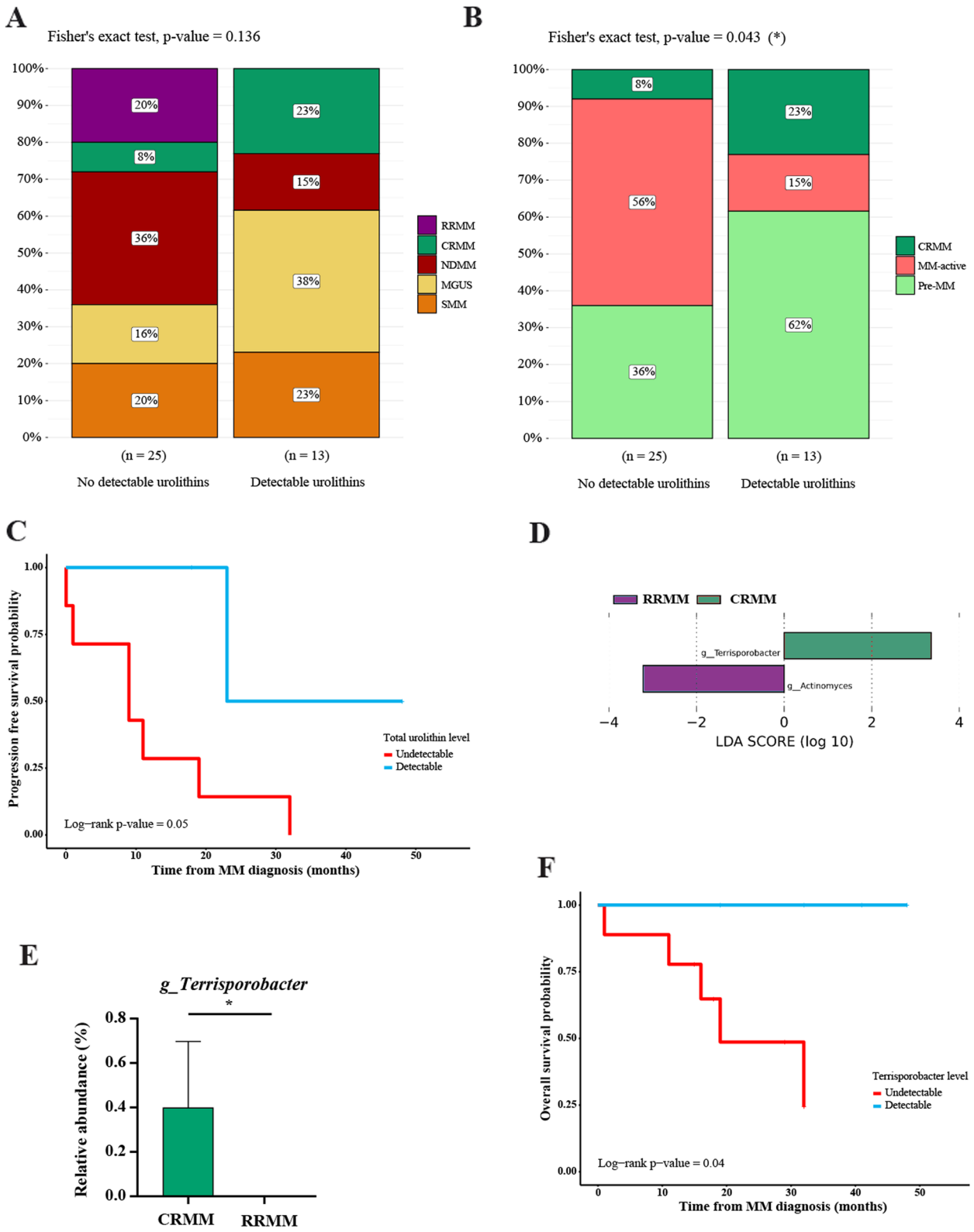

Fig. 1 (See legend on previous page.)

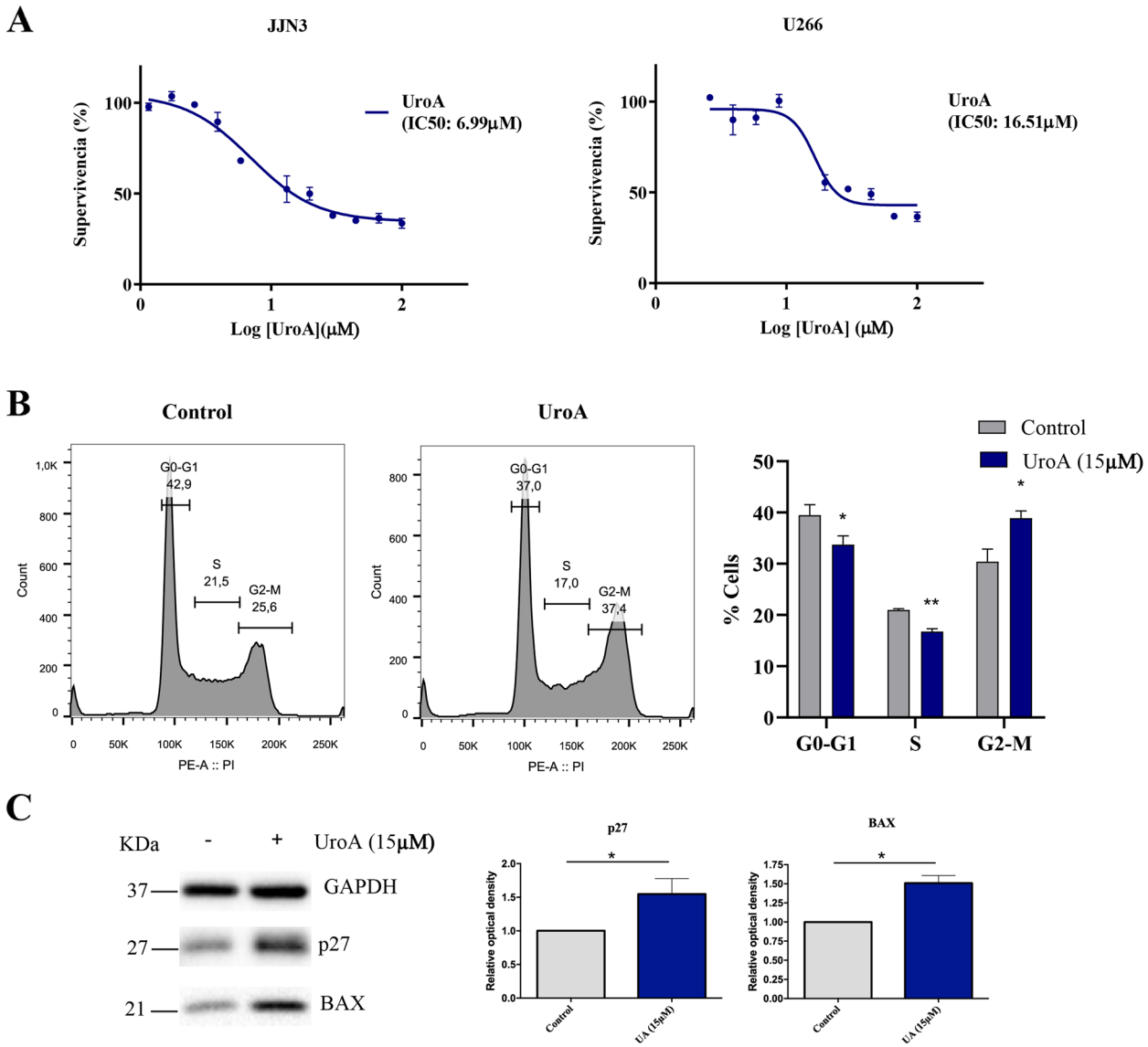

Fig. 2 **A** Dose–response curves of urolithin A (UroA) treatment in JJN3 and U266 cell lines after 48 h. The mean ± SEM of the data normalized to the control condition is shown. **B** Representation of the cell cycle in JJN3 cells after 24 h of exposure to UroA: the histogram shows the DNA content and cell count at the different stages of the cell cycle, and the bar chart shows the distribution by phases (G0/G1 phase, S phase, and G2/M phase). **C** Western blot analysis of the expression levels of p27 and BAX in untreated (control, DMSO) and treated JJN3 cells exposed to urolithin A (UroA) for 48 h. Bar graphs represent the mean ± SEM of the expression of the complexes normalized to the expression of glyceraldehyde 3-phosphate dehydrogenase (GAPDH) as a loading control. *$P \leq 0.05$

UroA exerts cytotoxic activity against primary myeloma cells ex vivo

We next tested the efficacy of UroA on primary plasma cells from patients with MM. Analysis revealed that exposure of CD38 + CD138 + plasma cells to UroA at 15 µM and 30 µM resulted in a decrease in viability (Fig. 4A, B), without affecting PBMCs or T cells from healthy donors (Supplementary Fig. 5).

UroA treatment improves survival in an in vivo model of MM

To verify the efficacy and safety of urolithin treatment, we used an in vivo NSG immunodeficient mouse model of MM. Bioluminescence image analysis revealed that UroA treatment inhibited the proliferation of tumor cells as compared with the control group of mice (Fig. 5A, B), with significant differences in the

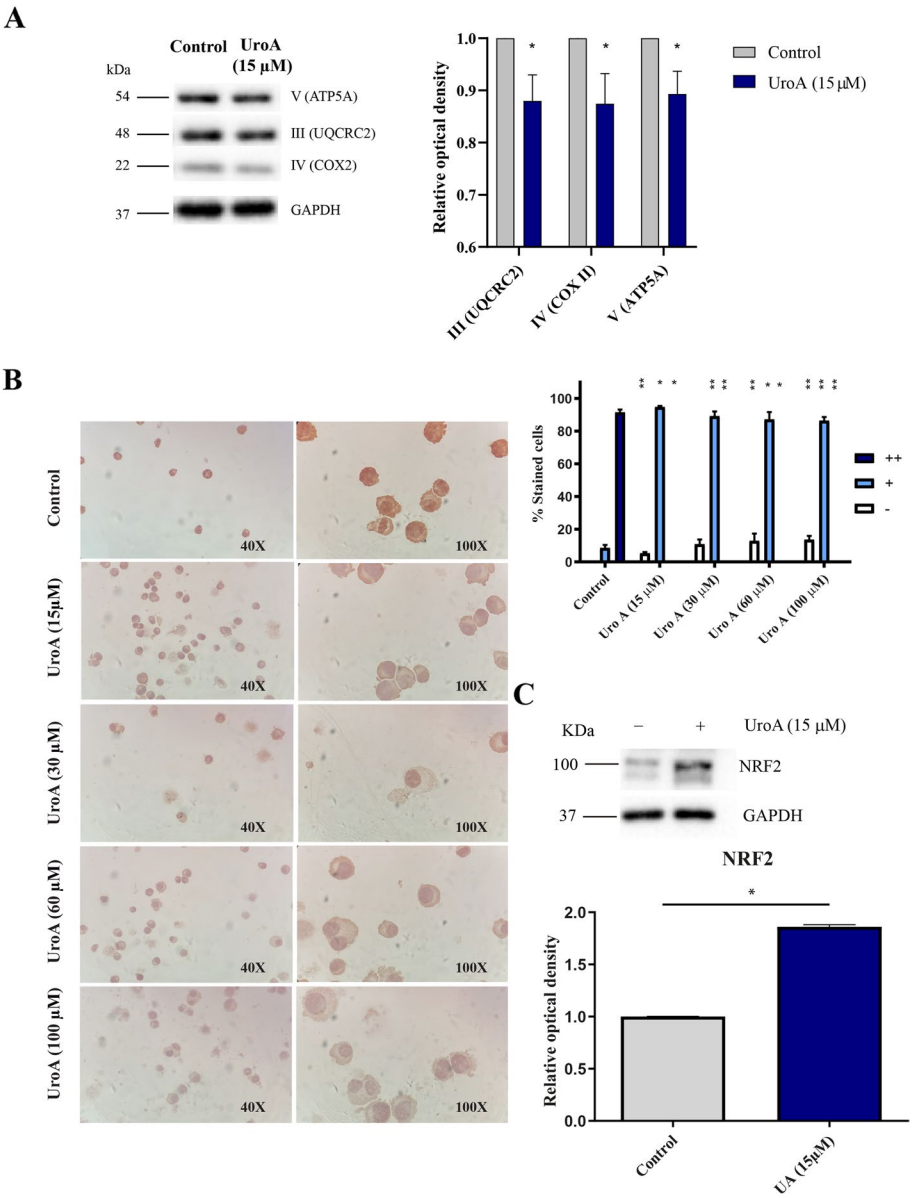

Fig. 3 **A** Western blot analysis of the expression levels of oxidative phosphorylation system complexes in untreated (control, DMSO) and treated JJN3 cells exposed to urolithin A (UroA) for 48 h. The complexes studied were as follows: NADH dehydrogenase beta subcomplex subunit 8 of complex I (NDUFB8), succinate dehydrogenase subunit B of complex II (SDHB), cytochrome c oxidase complex subunit 1 of complex IV (MTCO1), cytochrome b-c1 complex subunit 2 of complex III (UQCRC2), and ATP synthase subunit alpha of complex V (ATP5A). Bar graphs represent the mean ± SEM of the expression of the complexes normalized to the expression of glyceraldehyde 3-phosphate dehydrogenase (GAPDH) as a loading control. **B** Immunocytochemistry analysis of HNE adduction in JJN3 cells after exposure to DMSO or UroA at different concentrations for 48 h. Bar chart shows the percentage of stained (+ or + + levels of intensity) or non-stained (–) cells. **C** Western blot analysis of the expression levels of NRF2 in untreated (control, DMSO) and treated JJN3 cells exposed to urolithin A (UroA) for 48 h. Bar graphs represent the mean ± SEM of the expression of the complexes normalized to the expression of glyceraldehyde 3-phosphate dehydrogenase (GAPDH) as a loading control. *$P \leq 0.05$; **$P \leq 0.01$

overall survival of mice ($P = 0.0048$) (Fig. 5C). Specifically, the median survival for the treatment group was 29 days compared with 24.8 days for the control group. No signs of toxicity were evident at the doses employed. The UroA analysis in serum confirmed its absence (or the absence of its conjugates) in all the control mice and its presence (or the presence of its conjugates) in all the treated mice studied.

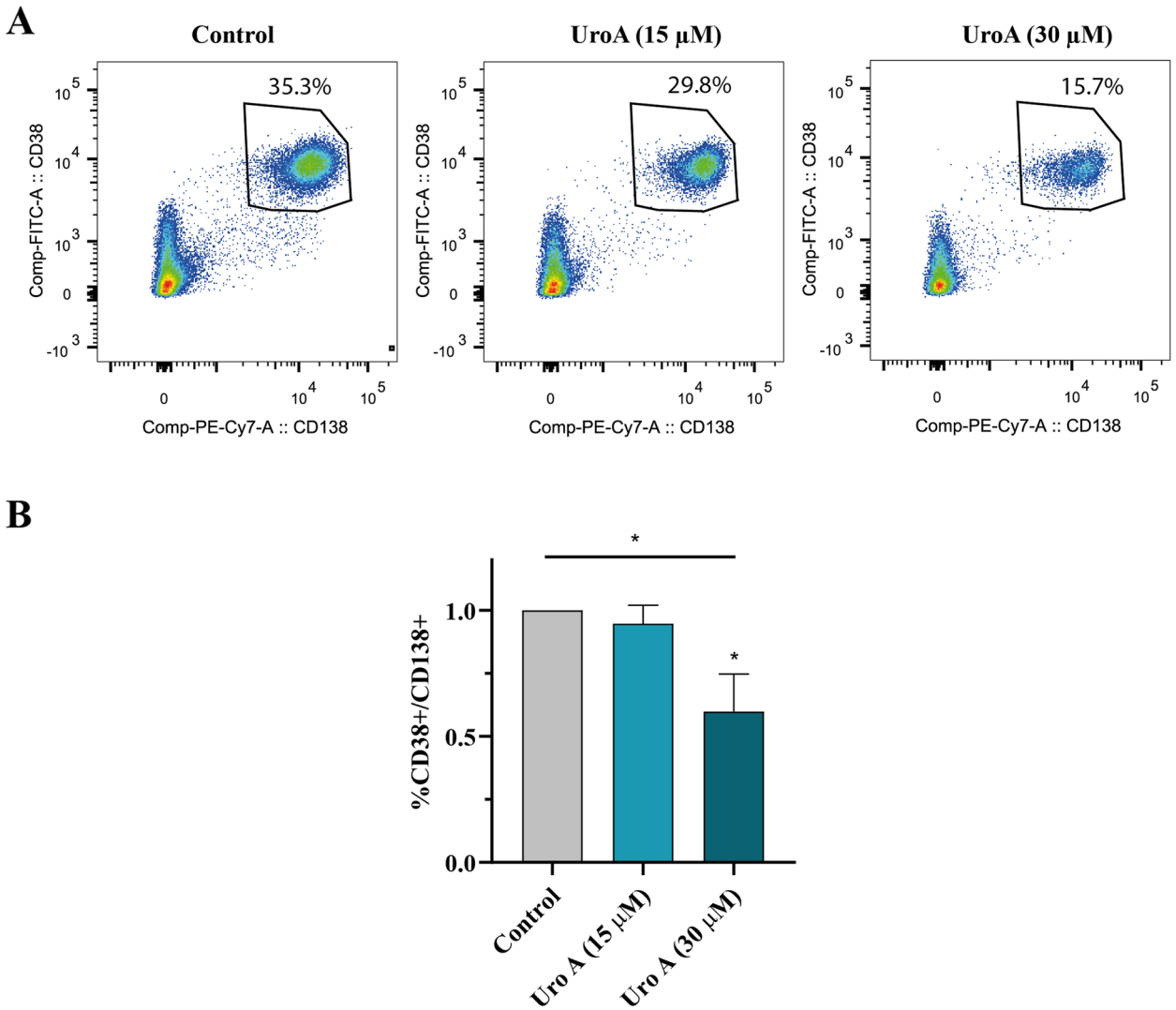

Fig. 4 **A** Representative dot plots showing changes in the plasma cell population upon 48-h exposure to urolithin A (UroA) at 15 µM ($n=5$) or 30 µM ($n=2$). Numbers represent the proportion of CD38 and CD138 positive cells. **B** Bar chart shows the mean of CD38/CD138 positive cells ± SEM populations in all patients analyzed normalized against the vehicle control. *$P \leq 0.05$

The combination of UroA and bortezomib has a synergistic effect against MM cells and modulates cancer-related pathways

Given the efficacy of UroA treatment on MM cell lines, we assessed the possible effect of its combination with bortezomib. Dose–response studies using the JJN3 line revealed that combination therapy had a synergistic effect at nearly all doses, with most of the CIs < 0.5 (Supplementary Fig. 3A). To assess the efficacy of urolithin in bortezomib-resistant cells, we performed a dose–response study in the resistant cell line JJN3_R-Btz, which had a 3.2-fold higher IC_{50} than equivalent bortezomib-sensitive cells. The cytotoxic effect of UroA treatment was similar in both cell types (Supplementary Fig. 3B), and the synergistic effect observed in the sensitive line was maintained in the bortezomib-resistant line (Supplementary Fig. 3C).

As we previously observed that UroA exerted a cell cycle effect, we investigated the main pathway involved in this process, the p53/p21 pathway, which is deregulated in MM [48]. We found that UroA and bortezomib as monotherapy had a similar effect on p53 protein expression in JJN3 cells, with both drugs slightly increasing the expression of p53 with respect to the control condition (Supplementary Fig. 4A). Notably, combination treatment significantly increased p53 expression ($P=0.05$). Furthermore, combination treatment increased p53 expression in JJN3_R-Btz cells ($P=0.05$) (Supplementary

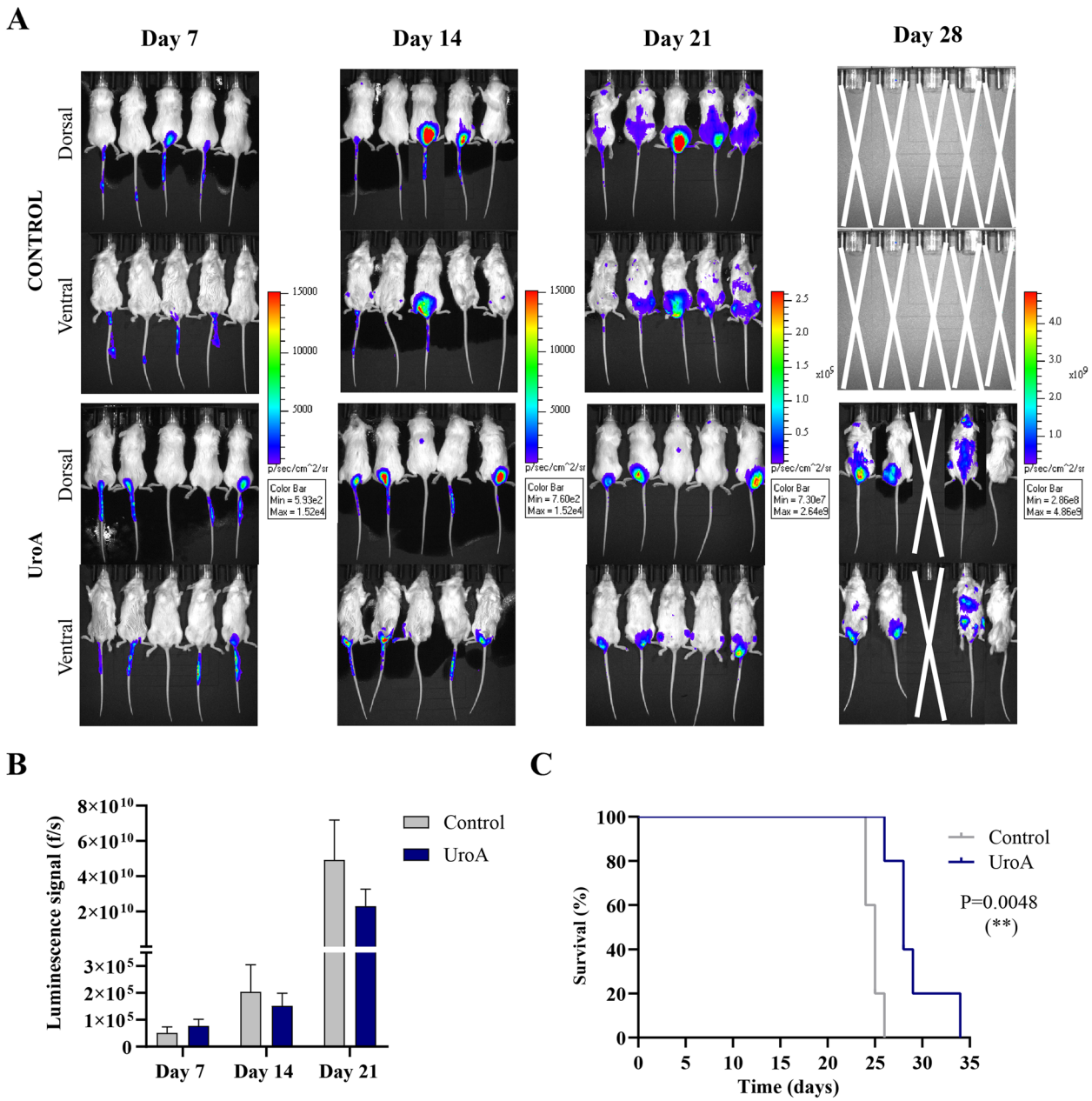

Fig. 5 **A** Bioluminescence analysis in dorsal and ventral position of the urolithin A (UroA)-treated group and the control group exposed to DMSO, after 7, 14, 21, and 28 days from the start of the experiment. **B** Comparison of the luminescent signal between the control and UroA-treated groups at days 7, 14, and 21. The mean ± SEM luminescent signal obtained in photons per second (f/s) is plotted. **C** Kaplan–Meier survival analysis of the control and UroA-treated groups. $^{**}P \leq 0.01$

Fig. 4A). Similar results were observed for its target p21, as combination treatment increased the level of expression in both bortezomib-sensitive and -resistant lines (both $P=0.05$) (Supplementary Fig. 4B). These results suggest that the combination UroA and bortezomib is effective in restoring the function of the p53 and p21 proteins.

Finally, we studied a second major pathway that contributes to the pathogenesis of MM, the PI3K/Akt/mTOR pathway. Exposure to UroA in monotherapy and in combination with bortezomib decreased p-mTOR levels in bortezomib-sensitive JJN3 cells, with significant differences with respect to controls (both $P=0.05$). In the bortezomib-resistant cell line, the combination

also resulted in a significant decrease in p-mTOR levels ($P=0.05$) (Supplementary Fig. 4C).

Moreover, we confirm UroA synergy with lenalidomide and venetoclax (Supplementary Fig. 6).

Discussion

We show that the levels of urolithins, including UroA, are positively associated with non-active MM disease and with prolonged survival in patients treated for the disease. UroA inhibited MM cell proliferation in vitro and ex vivo and increased survival in an in vivo model of the disease. This effect was likely mediated by cell cycle arrest, restoration of p53 and p21 expression, modulation of mitochondrial activity and oxidative stress, and reduction of mTOR phosphorylation.

The majority of patients with active disease in our cohort had no detectable levels of urolithin in the fecal and serum samples. As urolithin is metabolized into phase II conjugates, we have measured urolithin glucuronide and sulfates as well as the aglycones. To exclude the possible effect of age on urolithin production [49], we included controls in the same age range as the patients ($P=0.87$), allowing us to reject age as a determinant of urolithin production, as suggested by a previous study [50]. We also observed that patients without detectable urolithin in stool had worse progression-free survival, suggesting a protective effect of this metabolite.

We found a higher alpha diversity in urolithin-producing patients, as has been observed in other diseases [44, 51]. This increased richness and diversity of the gut microbiota might be related to a superior ability to convert dietary precursors into urolithins such as UroA. Although the composition of the microbiota is known to regulate the ability to produce UroA from its precursors, not all the bacteria responsible for this conversion are known [23]. Some urolithin-producing genera have been previously identified, such as *Ellagibacter* and *Gordonibacter* [52, 53]. However, they were not found to be biomarkers of controls *versus* MM in the present study, in contrast to other genera from the same family (Eggerthellaceae) such as *Raoultibacter*, *Senegalimassilia*, and *Adlercreutzia* (previously named *Enterorhabdus)* [53], which are indeed biomarkers of active MM. This might suggest that these genera are also involved in the production of urolithins, but further studies are needed to validate this hypothesis. Interestingly, one of the genera previously correlated with a greater ability to produce different urolithins [46, 47], *Terrisporobacter*, showed not only a decrease in its relative abundance in patients with relapsed and/or refractory disease but also a positive association with complete remission. In addition, the absence of *Terrisporobacter* was associated with worse progression-free survival. Strains of this genus could be potential probiotics with beneficial effects in MM, but more research is needed to confirm their safety before they can be considered as possible next-generation probiotics.

Based on these findings and given the evidence for the beneficial role of urolithins, particularly UroA, in numerous diseases [23], we investigated the effect of UroA in MM. Following a landmark in vitro study reporting the beneficial effects of urolithins on colon cancer cells in 2009 [31], their anticancer properties including anti-proliferation and promotion of antiangiogenesis have been explored in other cancer cell models including prostate, breast, kidney, liver, and brain cancer [54]. In the present study, we demonstrate the antiproliferative effects of UroA in MM in vitro, ex vivo, and in vivo.

UroA inhibited cell growth, achieving IC_{50} values of 6 and 16.51 µM in the MM cell lines JJN3 and U266, respectively. This inhibitory effect appears to be slightly greater than that observed in other tumorigenic lines, such as colorectal cancer, where IC_{50} values of 20–76 µM have been reported [29, 55, 56], or prostate cancer, with IC_{50} values of 32–70 µM [57]. As expected, UroA also affected the cell cycle in MM cells. Similar to other cancers, dysregulation of cell cycle proteins is common in MM, resulting in aberrant cycles of cell division that contribute to pathogenesis. Accordingly, inhibitors that induce cell cycle arrest are of great therapeutic interest [58]. Indeed, many anticancer agents, such as bendamustine and bortezomib, induce cell cycle arrest at key checkpoints. Both drugs are used to treat MM and induce arrest in the G2/M phase [59, 60]. In the present study, UroA treatment resulted in a depletion of cells in the G0/G1 phase with an accumulation of cells in the S and G2/M phases, demonstrating cell cycle arrest by p21 and p27 induction. Previous studies have reported that UroA induces cell cycle arrest in the G2/M phase in bladder cancer cells [61], prostate cancer cells [62], and in the G2/M and S phase in colon cancer cells [29], increasing apoptosis and cell death.

Malignant plasma cells exhibit altered mitochondrial metabolism, a well-characterized biological mechanism in the context of apoptosis [63]. Indeed, we previously demonstrated an increase in mitochondrial activity in plasma cells from patients with MM as the disease progresses [28]. One of the most consistent and well-studied mechanisms of action of UroA is its promotion of mitochondrial recycling (mitophagy) and maintenance of mitochondrial health [23]. Moreover, blocking mitochondrial metabolism in MM cells, thereby inhibiting mitochondrial activity, might have a major impact on slowing disease progression [28]. As expected, our results revealed that UroA affected mitochondrial oxidative phosphorylation chain complexes, with a

significant decrease in complexes COXII, ATP complex 5 alpha subunit ATP synthase (ATP5A), and UQCRC2. Our results are consistent with a previous study from our laboratory [28] examining the effect of a new mitochondrial inhibitor as a treatment for MM.

We also observed lower levels of oxidative stress in MM cells after exposure to UroA, as previously demonstrated in human bladder cancer T24 cells [64] and HepG2 liver cancer cells [65]. As the oncogenic transformation of plasma cells leads to enhanced oxidative stress, the attenuation of this phenomenon by UroA might reduce their malignant transformation [66]. Although antioxidants have a dual role in the context of cancer, they have long been considered tumor suppressors [66]. In addition, oxidative stress is generated as a by-product of increased mitochondrial respiration, as high levels of ATP are required to maintain the protein folding machinery, which is a highly ATP-dependent process [67]. Therefore, the reduced oxidative stress might also be related to the previously observed effect of UroA on mitochondrial function. In addition to exerting its effects through mitochondrial modulation, UroA also demonstrates an antioxidant role via the NRF2 pathway [68], as observed in our study.

Several studies have reported the antitumor activity of urolithins in cell lines of various cancers (reviewed in [52]). Furthermore, in vivo studies have shown that UroA administration increases survival in mouse models of acute kidney disease [69] and pancreatic cancer [30]. Our findings reveal for the first time that UroA treatment significantly increases survival in an MM mouse model. Importantly, after 28 days of follow-up, 4 out of 5 mice in the treatment group were still alive, while all mice in the untreated group died. In line with the study by Totiger et al. in pancreatic cancer [30], bioluminescence signal monitoring showed a reduction in tumor progression after UroA treatment.

One of the most commonly used drugs for the treatment of MM is bortezomib [70], whose mechanism of apoptosis induction via proteasome inhibition in MM results in changes in mitochondrial function [71]. Furthermore, in the context of resistance, metabolic regulatory proteins and mitochondrial redox homeostasis have been shown to be involved in the adaptation of myeloma cells to bortezomib [72]. In vitro analysis in MM lines treated with combination UroA and bortezomib revealed a synergistic effect of both compounds in both bortezomib-sensitive and -resistant lines. In addition, UroA was effective in both lines, which suggests that UroA in monotherapy or in combination could be a good therapeutic option in bortezomib-resistant patients. As UroA is a natural and nontoxic compound, it might allow lower doses of bortezomib to achieve therapeutic results with reduced toxicity.

Analysis of the signaling pathways that may be influenced by the combination of both compounds revealed that treatment with UroA and bortezomib increased p53 and p21 expression in both bortezomib-sensitive and -resistant lines. Dysregulation of the p53/p21 pathway is often evident in MM, and the approach to study it therapeutically has been extensively described [48]. In addition, p21 is an important cell cycle inhibitor [73], and so the increase in its expression would be related to the evident cell cycle arrest. Enhanced p53 and p21 expression levels after UroA treatment have previously been demonstrated in other tumoral cell lines [48]. In the present study, in addition to demonstrating that UroA increases p53 and p21 expression in an MM cell line, we also observed that combination with bortezomib potentiated this increase, not only in sensitive cells but also in resistant cells, which could be explained by their common action on the cell cycle.

Another important signaling pathway in MM tumor progression is the PI3K/Akt/mTOR pathway [74]. Numerous studies have reported that phosphorylated (active) mTOR might contribute to carcinogenesis [75–77], and much effort has been focused on mTOR inhibitors in the treatment of MM [78]. In the present study, UroA treatment inhibited the expression of phosphorylated mTOR, which was bolstered when combined with bortezomib. Thus, our results support the hypothesis proposed by Totiger et al. [30] that UroA down-regulates PI3K/Akt/mTOR oncogenic pathway signaling.

Moreover, in this work, UroA presented a synergistic effect with two other drugs: lenalidomide and venetoclax. There are several studies that demonstrate a beneficial role of urolithins with anticancer drugs. For example, using in vitro models, UroA potentiates 5-fluorouracil [79, 80] and oxaliplatin [50] in colon cancer, paclitaxel in esophageal carcinoma [81], and anti-PD1 therapy in pancreatic ductal adenocarcinoma [82]. Moreover, UroA enhanced the therapeutic effects of chemotherapy in xenograft models of gastric cancer [83] and pancreatic adenocarcinoma [30].

While our study provides valuable insights into the potential role of urolithins in the context of MM and the associated gut microbiota, several limitations should be acknowledged. The sample size of our clinical cohort, although diverse in MM stages, was relatively modest. A larger and more diverse patient population including more patients for ex vivo studies would increase the generalizability of our findings. Also, investigating the synergistic effects of UroA with other anti-myeloma agents, beyond bortezomib, might provide a more comprehensive understanding of its therapeutic potential.

In sum, our results show that natural compounds produced by microbiota such as urolithin could be very active against pathological plasma cells. Accordingly, urolithin might be promising therapeutic agent to prevent monoclonal gammopathy progression to MM or when used in the context of drug resistance when applied in combination.

Supplementary Information

The online version contains supplementary material available at https://doi.org/10.1186/s40168-025-02045-6.

Supplementary Material 1: Appendix 1. Clinical data of patients at different multiple myeloma stages and healthy control subjects.

Supplementary Material 2: Appendix 2. Relative abundance of operational taxonomic units (OTUs) across taxonomic ranks, including phylum, class, order, family, genus, and species, in patients at different multiple myeloma stages and healthy control subjects.

Supplementary Material 3: Appendix 3. Bioinformatics pipeline used for processing raw sequencing data into OTU tables.

Supplementary Material 4: Figure 1. A) Proportion (%) of patients with monoclonal gammopathy of undetermined significance (MGUS), smoldering myeloma (SMM), new diagnosed MM (NDMM), MM in complete remission (CRMM) and at relapse/refractory (RRMM) with detectable or undetectable levels of urolithin A in serum. B) Proportion (%) of patients with pre-malignant disease (MGUS and SMM), active-MM (NDMM and RRMM) and CRMM with detectable or undetectable levels of urolithin A in serum. C) Alpha-diversity measured by Chao1, D) Shannon and E) Simpson and F) Pielou indices in all patients that show differences between urolithin producers and non-producers. $^{**}P \leq 0.01$, $^{***}P \leq 0.001$. Supplementary Figure 2. A) Taxonomic biomarkers identified by linear discriminant analysis (LDA) effect size (LEfSE) analysis showing differences among multiple myeloma at diagnosis (NDMM) versus control (C) patients, and versus monoclonal gammopathy of undetermined significance (MGUS). B) Relative abundance (%) of the genera *Raoultibacter* and *Erysipelatoclostridium* in the progression of disease, from healthy controls (C), MGUS, smoldering multiple myeloma (SMM) and NDMM. C) Relative abundance of genera *Ruminococcus* and *Phocea* in NDMM and patients with relapse/refractory disease (RRMM). The results are represented by mean±SEM. $^{*}P \leq 0.05$, $^{**}P \leq 0.01$. Supplementary Figure 3. A) Normalized isobologram representing combination indices after the treatment with urolithin A and bortezomib in the JJN3 cell line. B) Dose-response curves after 48 hours of exposure to urolithin A in the sensitive JJN3 and resistant JJN3_R-Btz line. Mean ± SEM of data normalized to the control condition is represented. C) Normalized isobologram representing the combination indices after combination treatment with urolithin A and bortezomib in the JJN3_R-Btz line. Btz, bortezomib. Supplementary Figure 4. A) p53 levels analyzed by Western blot in the bortezomib (Btz) sensitive and resistant JJN3 cell line after exposure to urolithin A (UroA) at 15 µM, Btz at 4 nM and the combination of both (UroA+Btz) for 48 hours. B) p21 expression analyzed by qPCR in the Btz sensitive and resistant JJN3 cell line after exposure to UroA at 15 µM, Btz at 4 nM and the combination of both (UroA+Btz) for 48 hours. C) Expression levels of mTOR and p-mTOR analyzed by Western blot in Btz sensitive and resistant JJN3 cell line after exposure to UroA at 15 µM, Btz at 4 nM and the combination of both (UroA+Btz) for 3 hours. (A-C) The control condition was DMSO under the same conditions as the combination treatment. Bar graphs represent mean ± SEM of expression normalized against the glyceraldehyde 3-phosphate dehydrogenase (GAPDH) loading control (A, C) or GUS housekeeping gene (B). $^{*}P \leq 0.05$; $^{**}P \leq 0.01$; $^{***}P \leq 0.001$. Supplementary Figure 5. A) Bar chart shows the mean ± SEM of survival percentage in PBMCs from healthy donors upon 48 h exposure to urolithin A (UroA) at 15 µM ($n=3$) or 30 µM ($n=3$). B) Bar chart shows the mean ± SEM of survival percentage in T-cells from healthy donors upon 48 h exposure to urolithin A (UroA) at 15 µM ($n=3$) or 30 µM ($n=3$). No significant differences were observed. Supplementary Figure 6. A) Normalized isobologram representing combination indices after the treatment with urolithin A and lenalidomide in the JJN3 cell line. B) Normalized isobologram representing the combination indices after combination treatment with urolithin A and venetoclax in the JJN3 cell line. Supplementary Table S1. Clinical characteristics of classified patients at each stage of the disease. Supplementary Table S2. Type of urolithin and the metabotype of patients and controls with detectable levels of urolithins in feces. Supplementary Table S3. Statistical significance *p*-values adjusted by Benjamini-Hochberg (BH) procedure for the genus taxa included in the study. Supplementary Table S4. List of primary and secondary antibodies used for Western blot analyses. The name and reference of the commercial company, the source and the dilution of use of the different antibodies used for protein expression are detailed. For the primary antibodies, the protein to which they are directed and the MW of the protein are also mentioned.

Acknowledgements
Not applicable.

Authors' contributions
ARG, JML and ML designed the research, analyzed data and wrote the initial manuscript draft. ARG performed experiments and edited the manuscript. RGV, RAP, AOR, MAN, MLM, PGR, MDFL and RGV contributed performing experiments. AA performed the bioinformatical analysis. PJ, NL, JSP, RA contributed with patient sample. DGG helped with the design and edited the manuscript. MVS and FTB helped with the design and the analysis of the research and edition of the manuscript. RA, JML and ML provided resources and financial support. All authors reviewed the manuscript.

Funding
This work was supported by Grant PID2021-123056OA-I00 funded by MCIN/AEI/10.13039/501100011033 and ERDF A way of making Europe, the Instituto de Investigación Hospital 12 de Octubre (imas12), CIBERONC, AECC (Accelerator Award and Ideas Semilla, IDEAS20014LINA), and the CRIS foundation. A. R. G. and R. G. V. were the recipient of a grant from the Sociedad Española de Hematología y Hemoterapia; R. G. V. holded a predoctoral fellowship (FPU) grant from the Ministry of Science, Innovation and Universities of Spain (FPU19/04933); and R. A. P. holds a grant from ISCIII/CDTI (PMPTA22/00088).

Data availability
All data generated or analyzed during this study are included in this published article and its Online Supplementary Appendix. All source data are available on the SRA database (NCBI) under study number PRJNA1043906.

Declarations

Ethics approval and consent to participate
The study was approved by the Hospital 12 de Octubre Ethical Committee (21/580), and all patients and donors provided written informed consent following the Declaration of Helsinki.

Consent for publication
Not applicable.

Competing interests
The authors declare no competing interests.

Received: 11 June 2024 Accepted: 21 January 2025
Published online: 28 February 2025

References

1. Kyle RA, Remstein ED, Therneau TM, Dispenzieri A, Kurtin PJ, Hodnefield JM, Larson DR, Plevak MF, Jelinek DF, Fonseca R, et al. Clinical course and prognosis of smoldering (asymptomatic) multiple myeloma. N Engl J Med. 2007;356:2582–90. https://doi.org/10.1056/NEJMoa070389.

2. McShane CM, Murray LJ, Engels EA, Landgren O, Anderson LA. Common community-acquired infections and subsequent risk of multiple myeloma: a population-based study: infections and multiple myeloma. Int J Cancer. 2014;134:1734–40. https://doi.org/10.1002/ijc.28479.
3. Bigot-Corbel E, Gassin M, Corre I, Le Carrer D, Delaroche O, Hermouet S. Hepatitis C virus (HCV) infection, monoclonal immunoglobulin specific for HCV core protein, and plasma-cell malignancy. Blood. 2008;112:4357–8. https://doi.org/10.1182/blood-2008-07-167569.
4. Li Y, Li Y, Zhang L, Li W. Hepatitis C virus infection and risk of multiple myeloma: evidence from a meta-analysis based on 17 case-control studies. J Viral Hepat. 2017;24:1151–9. https://doi.org/10.1111/jvh.12742.
5. Yan J, Wang J, Zhang W, Chen M, Chen J, Liu W. Solitary plasmacytoma associated with Epstein-Barr virus: a clinicopathologic, cytogenetic study and literature review. Ann Diagn Pathol. 2017;27:1–6. https://doi.org/10.1016/j.anndiagpath.2016.09.002.
6. Hermouet S, Corre I, Gassin M, Bigot-Corbel E, Sutton CA, Casey JW. Hepatitis C virus, human herpesvirus 8, and the development of plasma-cell leukemia. N Engl J Med. 2003;348:178–9. https://doi.org/10.1056/NEJM200301093480219.
7. Feron D, Charlier C, Gourain V, Garderet L, Coste-Burel M, Le Pape P, Weigel P, Jacques Y, Hermouet S, Bigot-Corbel E. Multiplexed infectious protein microarray immunoassay suitable for the study of the specificity of monoclonal immunoglobulins. Anal Biochem. 2013;433:202–9. https://doi.org/10.1016/j.ab.2012.10.012.
8. Linares M, Hermouet S. Editorial: the role of microorganisms in multiple myeloma. Front Immunol. 2022;13:960829. https://doi.org/10.3389/fimmu.2022.960829.
9. Rodríguez-García A, Mennesson N, Hernandez-Ibarburu G, Morales ML, Garderet L, Bouchereau L, Allain-Maillet S, Piver E, Marbán I, Rubio D, et al. Impact of viral hepatitis therapy in multiple myeloma and other monoclonal gammopathies linked to hepatitis B or C viruses. Haematologica. 2023. https://doi.org/10.3324/haematol.2023.283096.
10. Belkaid Y, Hand TW. Role of the microbiota in immunity and inflammation. Cell. 2014;157:121–41. https://doi.org/10.1016/j.cell.2014.03.011.
11. Hanahan D. Hallmarks of cancer: new dimensions. Cancer Discov. 2022;12:31–46. https://doi.org/10.1158/2159-8290.CD-21-1059.
12. Zhang B, Gu J, Liu J, Huang B, Li J. Fecal microbiota taxonomic shifts in Chinese multiple myeloma patients analyzed by quantitative polimerase chain reaction (QPCR) and 16S rRNA high-throughput sequencing. Med Sci Monit. 2019;25:8269–80. https://doi.org/10.12659/MSM.919988.
13. Calcinotto A, Brevi A, Chesi M, Ferrarese R, Garcia Perez L, Grioni M, Kumar S, Garbitt VM, Sharik ME, Henderson KJ, et al. Microbiota-driven interleukin-17-producing cells and eosinophils synergize to accelerate multiple myeloma progression. Nat Commun. 2018;9:4832. https://doi.org/10.1038/s41467-018-07305-8.
14. Jian X, Zhu Y, Ouyang J, Wang Y, Lei Q, Xia J, Guan Y, Zhang J, Guo J, He Y, et al. Alterations of gut microbiome accelerate multiple myeloma progression by increasing the relative abundances of nitrogen-recycling bacteria. Microbiome. 2020;8:74. https://doi.org/10.1186/s40168-020-00854-5.
15. Peled JU, Gomes ALC, Devlin SM, Littmann ER, Taur Y, Sung AD, Weber D, Hashimoto D, Slingerland AE, Slingerland JB, et al. Microbiota as predictor of mortality in allogeneic hematopoietic-cell transplantation. N Engl J Med. 2020;382:822–34. https://doi.org/10.1056/NEJMoa1900623.
16. Pianko MJ, Devlin SM, Littmann ER, Chansakul A, Mastey D, Salcedo M, Fontana E, Ling L, Tavitian E, Slingerland JB, et al. Minimal residual disease negativity in multiple myeloma is associated with intestinal microbiota composition. Blood Adv. 2019;3:2040–4. https://doi.org/10.1182/bloodadvances.2019032276.
17. Antoine Pepeljugoski C, Morgan G, Braunstein M. Analysis of intestinal microbiome in multiple myeloma reveals progressive dysbiosis compared to MGUS and healthy individuals. Blood. 2019;134:3076. https://doi.org/10.1182/blood-2019-130643.
18. Ahmed N, Ghannoum M, Gallogly M, de Lima M, Malek E. Influence of gut microbiome on multiple myeloma: friend or foe? J Immunother Cancer. 2020;8:e000576. https://doi.org/10.1136/jitc-2020-000576.
19 Uribe-Herranz M, Klein-González N, Rodríguez-Lobato LG, Juan M, Fernández de Larrea C. Gut microbiota influence in hematological malignancies: from genesis to cure. Int J Mol Sci. 2021;22:1026. https://doi.org/10.3390/ijms22031026.
20. Shah UA, Maclachlan KH, Derkach A, Salcedo M, Barnett K, Caple J, Blaslov J, Tran L, Ciardiello A, Burge M, et al. Sustained minimal residual disease negativity in multiple myeloma is associated with stool butyrate and healthier plant-based diets. Clin Cancer Res. 2022:OF1–OF7. https://doi.org/10.1158/1078-0432.CCR-22-0723.
21. Rodríguez-García A, Arroyo A, Garcia-Vicente R, Morales ML, Gómez-Gordo R, Justo P, Cuellar C, Sánchez-Pina J, López N, Alonso R, et al. Short-chain fatty acid production by gut microbiota predicts treatment response in multiple myeloma. Clin Cancer Res. 2023. https://doi.org/10.1158/1078-0432.CCR-23-0195.
22. Al-Harbi SA, Abdulrahman AO, Zamzami MA, Khan MI. Urolithins: the gut based polyphenol metabolites of ellagitannins in cancer prevention, a review. Front Nutr. 2021;8:647582. https://doi.org/10.3389/fnut.2021.647582.
23. D'Amico D, Andreux PA, Valdés P, Singh A, Rinsch C, Auwerx J. Impact of the natural compound urolithin A on health, disease, and aging. Trends Mol Med. 2021:S1471491421001180. https://doi.org/10.1016/j.molmed.2021.04.009.
24. Selma MV, Beltrán D, García-Villalba R, Espín JC, Tomás-Barberán FA. Description of urolithin production capacity from ellagic acid of two human intestinal Gordonibacter species. Food Funct. 2014;5:1779–84. https://doi.org/10.1039/C4FO00092G.
25. Zhang M, Cui S, Mao B, Zhang Q, Zhao J, Zhang H, Tang X, Chen W. Ellagic acid and intestinal microflora metabolite urolithin A: a review on its sources, metabolic distribution, health benefits, and biotransformation. Crit Rev Food Sci Nutr. 2022:1–23. https://doi.org/10.1080/10408398.2022.2036693.
26. Ryu D, Mouchiroud L, Andreux PA, Katsyuba E, Moullan N, Nicolet-dit-Félix AA, Williams EG, Jha P, Lo Sasso G, Huzard D, et al. Urolithin A induces mitophagy and prolongs lifespan in C. elegans and increases muscle function in rodents. Nat Med. 2016;22:879–88. https://doi.org/10.1038/nm.4132.
27. Luan P, D'Amico D, Andreux PA, Laurila P-P, Wohlwend M, Li H, Imamura de Lima T, Place N, Rinsch C, Zanou N, et al. Urolithin A improves muscle function by inducing mitophagy in muscular dystrophy. Sci Transl Med. 2021;13:319. https://doi.org/10.1126/scitranslmed.abb0319.
28. Ortiz-Ruiz A, Ruiz-Heredia Y, Morales ML, Aguilar-Garrido P, García-Ortiz A, Valeri A, Bárcena C, García-Martin RM, Garrido V, Moreno L, et al. Myc-related mitochondrial activity as a novel target for multiple myeloma. Cancers. 2021;13:1662. https://doi.org/10.3390/cancers13071662.
29. El-Wetidy MS, Ahmad R, Rady I, Helal H, Rady MI, Vaali-Mohammed M-A, Al-Khayal K, Traiki TB, Abdulla M-H. Urolithin A induces cell cycle arrest and apoptosis by inhibiting Bcl-2, increasing p53–p21 proteins and reactive oxygen species production in colorectal cancer cells. Cell Stress Chaperones. 2021;26:473–93. https://doi.org/10.1007/s12192-020-01189-8.
30. Totiger TM, Srinivasan S, Jala VR, Lamichhane P, Dosch AR, Gaidarski AA, Joshi C, Rangappa S, Castellanos J, Vemula PK, et al. Urolithin A, a novel natural compound to target PI3K/AKT/mTOR pathway in pancreatic cancer. Mol Cancer Ther. 2019;18:301–11. https://doi.org/10.1158/1535-7163.MCT-18-0464.
31. González-Sarrías A, Espín J-C, Tomás-Barberán FA, García-Conesa M-T. Gene expression, cell cycle arrest and MAPK signalling regulation in Caco-2 cells exposed to ellagic acid and its metabolites, urolithins. Mol Nutr Food Res. 2009;53:686–98. https://doi.org/10.1002/mnfr.200800150.
32. Bolyen E, Rideout JR, Dillon MR, Bokulich NA, Abnet CC, Al-Ghalith GA, Alexander H, Alm EJ, Arumugam M, Asnicar F, et al. Reproducible, interactive, scalable and extensible microbiome data science using QIIME 2. Nat Biotechnol. 2019;37:852–7. https://doi.org/10.1038/s41587-019-0209-9.
33. Callahan BJ, McMurdie PJ, Rosen MJ, Han AW, Johnson AJ, Holmes SP. DADA2: high-resolution sample inference from Illumina amplicon data. Nat Methods. 2016;13(7):581–3. https://doi.org/10.1038/nmeth.3869.
34. Quast C, Pruesse E, Yilmaz P, Gerken J, Schweer T, Yarza P, Peplies J, Glöckner FO. The SILVA ribosomal RNA gene database project: improved data processing and web-based tools. Nucleic Acids Res. 2013;41:D590–6. https://doi.org/10.1093/nar/gks1219.
35. Rognes T, Flouri T, Nichols B, Quince C, Mahé F. VSEARCH: a versatile open source tool for metagenomics. PeerJ. 2016;4:e2584. https://doi.org/10.7717/peerj.2584.

36. Segata N, Izard J, Waldron L, Gevers D, Miropolsky L, Garrett WS, Huttenhower C. Metagenomic biomarker discovery and explanation. Genome Biol. 2011;12(6):R60. https://doi.org/10.1186/gb-2011-12-6-r60.
37. García-Villalba R, Selma MV, Espín JC, Tomás-Barberán FA. Identification of novel urolithin metabolites in human feces and urine after the intake of a pomegranate extract. J Agric Food Chem. 2019;67:11099–107. https://doi.org/10.1021/acs.jafc.9b04435.
38. García-Villalba R, Espín JC, Tomás-Barberán FA. Chromatographic and spectroscopic characterization of urolithins for their determination in biological samples after the intake of foods containing ellagitannins and ellagic acid. J Chromatogr A. 2016;1428:162–75. https://doi.org/10.1016/j.chroma.2015.08.044.
39. Chou T-C. Drug combination studies and their synergy quantification using the Chou-Talalay method. Cancer Res. 2010;70:440–6. https://doi.org/10.1158/0008-5472.CAN-09-1947.
40. Livak KJ, Schmittgen TD. Analysis of relative gene expression data using real-time quantitative PCR and the 2−ΔΔCT method. Methods. 2001;25:402–8. https://doi.org/10.1006/meth.2001.1262.
41. Rodríguez-García A, Morales ML, Garrido-García V, García-Baquero I, Leivas A, Carreño-Tarragona G, Sánchez R, Arenas A, Cedena T, Ayala RM, et al. Protein carbonylation in patients with myelodysplastic syndrome: an opportunity for deferasirox therapy. Antioxidants. 2019;8:508. https://doi.org/10.3390/antiox8110508.
42. RStudio Team. RStudio: integrated development for R. Boston: RStudio, PBC. 2020. http://www.rstudio.com/.
43. Romo-Vaquero M, Cortés-Martín A, Loria-Kohen V, Ramírez-de-Molina A, García-Mantrana I, Collado MC, Espín JC, Selma MV. Deciphering the human gut microbiome of urolithin metabotypes: association with enterotypes and potential cardiometabolic health implications. Mol Nutr Food Res. 2019;63:1800958. https://doi.org/10.1002/mnfr.201800958.
44 Bilen M, Cadoret F, Dubourg G, Daoud Z, Fournier PE, Raoult D. 'Raoultibacter timonensis' gen. nov., sp. nov. , a new bacterium isolated from the human gut of a Pygmy woman. New Microbes New Infect. 2017;16:45–6. https://doi.org/10.1016/j.nmni.2016.12.016.
45. Meslier V, Laiola M, Roager HM, De Filippis F, Roume H, Quinquis B, Giacco R, Mennella I, Ferracane R, Pons N, et al. Mediterranean diet intervention in overweight and obese subjects lowers plasma cholesterol and causes changes in the gut microbiome and metabolome independently of energy intake. Gut. 2020;69:1258–68. https://doi.org/10.1136/gutjnl-2019-320438.
46. Iglesias-Aguirre CE, Romo-Vaquero M, Victoria Selma M, Carlos EJ. Unveiling metabotype clustering in resveratrol, daidzein, and ellagic acid metabolism: prevalence, associated gut microbiomes, and their distinctive microbial networks. Food Res Int Ott Ont. 2023;173:113470. https://doi.org/10.1016/j.foodres.2023.113470.
47. García-Mantrana I, Calatayud M, Romo-Vaquero M, Espín JC, Selma MV, Collado MC. Urolithin metabotypes can determine the modulation of gut microbiota in healthy individuals by tracking walnuts consumption over three days. Nutrients. 2019;11:2483. https://doi.org/10.3390/nu11102483.
48. Jovanović KK, Escure G, Demonchy J, Willaume A, Van de Wyngaert Z, Farhat M, Chauvet P, Facon T, Quesnel B, Manier S. Deregulation and targeting of TP53 pathway in multiple myeloma. Front Oncol. 2019;8. https://www.frontiersin.org/articles/10.3389/fonc.2018.00665. Accessed 15 Sept 2022.
49. Cortés-Martín A, García-Villalba R, González-Sarrías A, Romo-Vaquero M, Loria-Kohen V, Ramírez-de-Molina A, Tomás-Barberán FA, Selma MV, Espín JC. The gut microbiota urolithin metabotypes revisited: the human metabolism of ellagic acid is mainly determined by aging. Food Funct. 2018;9:4100–6. https://doi.org/10.1039/c8fo00956b.
50. Tomás-Barberán FA, García-Villalba R, González-Sarrías A, Selma MV, Espín JC. Ellagic acid metabolism by human gut microbiota: consistent observation of three urolithin phenotypes in intervention trials, independent of food source, age, and health status. J Agric Food Chem. 2014;62:6535–8. https://doi.org/10.1021/jf5024615.
51. Romo-Vaquero M, Fernández-Villalba E, Gil-Martinez A-L, Cuenca-Bermejo L, Carlos Espín J, Trinidad Herrero M, Victoria SM. Urolithins: potential biomarkers of gut dysbiosis and disease stage in Parkinson's patients. Food Funct. 2022;13:6306–16. https://doi.org/10.1039/D2FO00552B.
52. Iglesias-Aguirre CE, García-Villalba R, Beltrán D, Frutos-Lisón MD, Espín JC, Tomás-Barberán FA, Selma MV. Gut bacteria involved in ellagic acid metabolism to yield human urolithin metabotypes revealed. J Agric Food Chem. 2023;71:4029–35. https://doi.org/10.1021/acs.jafc.2c08889.
53. Iglesias-Aguirre CE, González-Sarrías A, Cortés-Martín A, Romo-Vaquero M, Osuna-Galisteo L, Cerón JJ, Espín JC, Selma MV. In vivo administration of gut bacterial consortia replicates urolithin metabotypes A and B in a non-urolithin-producing rat model. Food Funct. 2023;14:2657–67. https://doi.org/10.1039/d2fo03957e.
54 García-Villalba R, Tomás-Barberán FA, Iglesias-Aguirre CE, Giménez-Bastida JA, González-Sarrías A, Selma MV, Espín JC. Ellagitannins, urolithins, and neuroprotection: human evidence and the possible link to the gut microbiota. Mol Aspects Med. 2022;89:101109. https://doi.org/10.1016/j.mam.2022.101109.
55. González-Sarrías A, García-Villalba R, Romo-Vaquero M, Alasalvar C, Örem A, Zafrilla P, Tomás-Barberán FA, Selma MV, Espín JC. Clustering according to urolithin metabotype explains the interindividual variability in the improvement of cardiovascular risk biomarkers in overweight-obese individuals consuming pomegranate: a randomized clinical trial. Mol Nutr Food Res. 2017;61. https://doi.org/10.1002/mnfr.201600830.
56. Norden E, Heiss EH. Urolithin A gains in antiproliferative capacity by reducing the glycolytic potential via the p53/TIGAR axis in colon cancer cells. Carcinogenesis. 2019;40:93–101. https://doi.org/10.1093/carcin/bgy158.
57. Dahiya NR, Chandrasekaran B, Kolluru V, Ankem M, Damodaran C, Vadhanam MV. A natural molecule, urolithin A, downregulates androgen receptor activation and suppresses growth of prostate cancer. Mol Carcinog. 2018;57:1332–41. https://doi.org/10.1002/mc.22848.
58. Maes A, Menu E, Veirman KD, Maes K, Vand erkerken K, De Bruyne E. The therapeutic potential of cell cycle targeting in multiple myeloma. Oncotarget. 2017;8:90501–20. https://doi.org/10.18632/oncotarget.18765.
59. Gaul L, Mandl-Weber S, Baumann P, Emmerich B, Schmidmaier R. Bendamustine induces G2 cell cycle arrest and apoptosis in myeloma cells: the role of ATM-Chk2-Cdc25A and ATM-p53-p21-pathways. J Cancer Res Clin Oncol. 2008;134:245–53. https://doi.org/10.1007/s00432-007-0278-x.
60. Hong YS, Hong S-W, Kim S-M, Jin D-H, Shin J-S, Yoon DH, Kim K-P, Lee J-L, Heo DS, Lee JS, et al. Bortezomib induces G2-M arrest in human colon cancer cells through ROS-inducible phosphorylation of ATM-CHK1. Int J Oncol. 2012;41:76–82. https://doi.org/10.3892/ijo.2012.1448.
61. Liberal J, Carmo A, Gomes C, Cruz MT, Batista MT. Urolithins impair cell proliferation, arrest the cell cycle and induce apoptosis in UMUC3 bladder cancer cells. Invest New Drugs. 2017;35:671–81. https://doi.org/10.1007/s10637-017-0483-7.
62. Vicinanza R, Zhang Y, Henning SM, Heber D. Pomegranate juice metabolites, ellagic acid and urolithin A, synergistically inhibit androgen-independent prostate cancer cell growth via distinct effects on cell cycle control and apoptosis. Evid Based Complement Alternat Med. 2013;2013:e247504. https://doi.org/10.1155/2013/247504.
63. Dalton WS. Targeting the mitochondria: an exciting new approach to myeloma therapy. Commentary re: N. J. Bahlis et al., Feasibility and correlates of arsenic trioxide combined with ascorbic acid-mediated depletion of intracellular glutathione for the treatment of relapsed/refractory multiple myeloma. Clin. Cancer Res., 8: 3658-3668, 2002. Clin Cancer Res Off J Am Assoc Cancer Res. 2002;8:3658–68.
64. Qiu Z, Zhou B, Jin L, Yu H, Liu L, Liu Y, Qin C, Xie S, Zhu F. In vitro antioxidant and antiproliferative effects of ellagic acid and its colonic metabolite, urolithins, on human bladder cancer T24 cells. Food Chem Toxicol Int J Publ Br Ind Biol Res Assoc. 2013;59:428–37. https://doi.org/10.1016/j.fct.2013.06.025.
65. Wang Y, Qiu Z, Zhou B, Liu C, Ruan J, Yan Q, Liao J, Zhu F. In vitro antiproliferative and antioxidant effects of urolithin A, the colonic metabolite of ellagic acid, on hepatocellular carcinomas HepG2 cells. Toxicol Vitro Int J Publ Assoc BIBRA. 2015;29:1107–15. https://doi.org/10.1016/j.tiv.2015.04.008.
66. Lipchick BC, Fink EE, Nikiforov MA. Oxidative stress and proteasome inhibitors in multiple myeloma. Pharmacol Res. 2016;105:210–5. https://doi.org/10.1016/j.phrs.2016.01.029.
67. Murphy MP. How mitochondria produce reactive oxygen species. Biochem J. 2009;417:1–13. https://doi.org/10.1042/BJ20081386.
68. Gao Z, Yi W, Tang J, Sun Y, Huang J, Lan T, Dai X, Xu S, Jin ZG, Wu X. Urolithin A protects against acetaminophen-induced liver injury in mice via sustained activation of Nrf2. Int J Biol Sci. 2022;18(5):2146–62. https://doi.org/10.7150/ijbs.69116.

69. Zou D, Ganugula R, Arora M, Nabity MB, Sheikh-Hamad D, Kumar MNVR. Oral delivery of nanoparticle urolithin A normalizes cellular stress and improves survival in mouse model of cisplatin-induced AKI. Am J Physiol Renal Physiol. 2019;317:F1255–64. https://doi.org/10.1152/ajprenal.00346.2019.
70. Jayaweera SPE, Wanigasinghe Kanakanamge SP, Rajalingam D, Silva GN. Carfilzomib: a promising proteasome inhibitor for the treatment of relapsed and refractory multiple myeloma. Front Oncol. 2021;11. https://www.frontiersin.org/article/10.3389/fonc.2021.740796. Accessed 29 June 2022.
71. Chauhan D, Li G, Podar K, Hideshima T, Mitsiades C, Schlossman R, Munshi N, Richardson P, Cotter FE, Anderson KC. Targeting mitochondria to overcome conventional and bortezomib/proteasome inhibitor PS-341 resistance in multiple myeloma (MM) cells. Blood. 2004;104:2458–66. https://doi.org/10.1182/blood-2004-02-0547.
72. Soriano GP, Besse L, Li N, Kraus M, Besse A, Meeuwenoord N, Bader J, Everts B, den Dulk H, Overkleeft HS, et al. Proteasome inhibitor-adapted myeloma cells are largely independent from proteasome activity and show complex proteomic changes, in particular in redox and energy metabolism. Leukemia. 2016;30:2198–207. https://doi.org/10.1038/leu.2016.102.
73. Kreis N-N, Louwen F, Yuan J. Less understood issues: p21(Cip1) in mitosis and its therapeutic potential. Oncogene. 2015;34:1758–67. https://doi.org/10.1038/onc.2014.133.
74. Hu J, Hu W-X. Targeting signaling pathways in multiple myeloma: pathogenesis and implication for treatments. Cancer Lett. 2018;414:214–21. https://doi.org/10.1016/j.canlet.2017.11.020.
75. van der Hage JA, van den Broek LJCM, Legrand C, Clahsen PC, Bosch CJA, Robanus-Maandag EC, van de Velde CJH, van de Vijver MJ. Overexpression of P70 S6 kinase protein is associated with increased risk of locoregional recurrence in node-negative premenopausal early breast cancer patients. Br J Cancer. 2004;90:1543–50. https://doi.org/10.1038/sj.bjc.6601741.
76. Hou G, Xue L, Lu Z, Fan T, Tian F, Xue Y. An activated mTOR/p70S6K signaling pathway in esophageal squamous cell carcinoma cell lines and inhibition of the pathway by rapamycin and siRNA against mTOR. Cancer Lett. 2007;253:236–48. https://doi.org/10.1016/j.canlet.2007.01.026.
77. Faried LS, Faried A, Kanuma T, Aoki H, Sano T, Nakazato T, Tamura T, Kuwano H, Minegishi T. Expression of an activated mammalian target of rapamycin in adenocarcinoma of the cervix: a potential biomarker and molecular target therapy. Mol Carcinog. 2008;47:446–57. https://doi.org/10.1002/mc.20402.
78. Calimeri T, Ferreri AJM. m-TOR inhibitors and their potential role in haematological malignancies. Br J Haematol. 2017;177:684–702. https://doi.org/10.1111/bjh.14529.
79. González-Sarrías A, Tomé-Carneiro J, Bellesia A, Tomás Barberán FA, Espín JC. The ellagic acid-derived gut microbiota metabolite urolithin A potentiates the anticancer effect of 5-fluorouracil chemotherapy in human colon cancer cells. Food Funct. 2015;6:1460–9. https://doi.org/10.1039/c5fo00120j.
80. Ghosh S, Singh R, Vanwinkle ZM, Guo H, Vemula PK, Goel A, Haribabu B, Jala VR. Microbial metabolite restricts 5-fluorouracil-resistant colonic tumor progression by sensitizing drug transporters via regulation of FOXO3-FOXM1 axis. Theranostics. 2022;12(12):5574–95. https://doi.org/10.7150/thno.70754.
81. Mirzaei S, Iranshahy M, Gholamhosseinian H, Matin MM, Rassouli FB. Urolithins increased anticancer effects of chemical drugs, ionizing radiation and hyperthermia on human esophageal carcinoma cells in vitro. Tissue Cell. 2022;77:101846. https://doi.org/10.1016/j.tice.2022.101846.
82. Mehra S, Garrido VT, Dosch AR, Lamichhane P, Srinivasan S, Singh SP, Zhou Z, De Castro SI, Joshi C, Ban Y, Datta J, Gilboa E, Merchant NB, Nagathihalli NS. Remodeling of stromal immune microenvironment by urolithin A improves survival with immune checkpoint blockade in pancreatic cancer. Cancer Res Commun. 2023;3(7):1224–36. https://doi.org/10.1158/2767-9764.CRC-22-0329.
83. Zhang Y, Jiang L, Su P, Yu T, Ma Z, Liu Y, Yu J. Urolithin A suppresses tumor progression and induces autophagy in gastric cancer via the PI3K/Akt/mTOR pathway. Drug Dev Res. 2023;84(2):172–84. https://doi.org/10.1002/ddr.22021.

Publisher's Note